A Pathway Switching Mechanism for Water Catalyzed Ethanol Decomposition on Cu(111)

Robert H. Wells[a] *and Rex T. Skodje* [a*]

[a]Department of Chemistry, University of Colorado, Boulder, CO 80309-0215

Abstract: A first-principles study of the ethanol decomposition mechanism on Cu(111) is presented with a focus on the selectivity of acetaldehyde production controlled through the addition of molecular water in the reaction network. We include a pathway switching bimolecular mechanism in which water and a substrate species undergo a double hydrogen exchange reaction which alters the decomposition pathway of ethanol. The mechanistic study is performed on a portion of the ethanol decomposition network consisting of eight hydrogen abstraction reactions, adsorption of ethanol, desorption of acetaldehyde, and addition of two water catalyzed pathway switching reactions. The reaction rates are determined with density functional theory (DFT) and transition state theory (TST). We use a recently developed technique, the sum over histories representation (SOHR), to describe the chemical pathways of ethanol decomposition. The addition of the water pathway switching mechanism shows an increase of acetaldehyde production which closely follows experimental results.

1. Introduction

Determining realistic models that describe the heterogeneous catalysis of steam reformation processes of alcohols is a challenging problem.[1,2] The chemical mechanisms responsible for these systems can become quite large with dozens of elementary steps and intermediates involved. Many of these elementary processes are elusive to direct experimental observation. The use of density functional theory (DFT) is thus one of the most valuable tools in mapping out this chemistry since observables such as the turn over frequency (TOF) can be generated from a hypothetical mechanism.[3-5] One of the long-standing goals of heterogeneous catalysis is the efficient production of H_2 as an energy source for hydrogen fuel cells as well as conversion of H_2 back to storable fuel source.[6-8] Simple alcohols, such as methanol[9-12] and ethanol[13,14], have been shown to be useful sources of H_2 via methanol steam reforming (MSR) $CH_3OH+H_2O\rightarrow CO_2+3H_2$ and ethanol steam reforming (ESR) $CH_3CH_2OH+3H_2O\rightarrow 2CO_2+6H_2$, respectively. In the present work we focus on the ESR system which has been less well studied than the MSR problem. We note that ethanol chemistry on various catalytic surfaces has also been studied for ethyl acetate

synthesis[15] and the production of acetic acid[16,17] which are also relevant to the present work. Much of the effort on these problems has focused on the first few hydrogen-atom abstraction reactions from the alcohol and these steps trigger the subsequent chemistry and are crucial to the selectivity of the catalyst. In particular it has been of interest to access the relative efficiency of various catalytic metals and crystal faces on these initial steps.[18-23] It has been observed that Rh surfaces are particularly active although expensive for practical applications.[24] Copper surfaces, Cu(100) and Cu(111) are also active and may provide a less expensive alternative.[13,25] Experiments have demonstrated that Cu is more active in H_2 generation from ethanol than iron or nickel.[26] In the present work we explore the Cu(111) surface.

Figure 1 gives a detailed view of the individual reactions and molecular species that make up a significant fraction of the chemical network for ESR on Cu(111) of which H_2O and its derivatives are present (wet reformation). The network contains a large number of hydrogen abstractions and attachment reactions from various intermediates, together with a number of critical reactions involving the formation and breaking of C-C and C-O bonds. It is observed that a number of closed shell molecules lie *en route* to syngas formation. The gas phase production of these by-products will result in smaller amounts of H_2-production compared to full decomposition, i.e. $C_2H_5OH+2H_2O \rightarrow 2CO_2+5H_2$. While many of these by-products can be avoided by adjusting the reaction conditions, one that is not easy to avoid is acetaldehyde gas, $CH_3CHO(g)$.[27,28] It is clear from Fig. 1 that the formation of $CH_3CHO(g)$ occurs very early in the decomposition process. There are two simple reaction routes (or chemical pathways) from ethanol which directly lead to acetaldehyde: (1) $CH_3CH_2OH \rightarrow CH_3CH_2O + H \rightarrow CH_3CHO + 2H$ and (2) $CH_3CH_2OH \rightarrow CH_3CHOH + H \rightarrow CH_3CHO + 2H$. On the other hand, a different sequence of abstraction reactions would avoid the acetaldehyde intermediate, e.g. $CH_3CH_2OH \rightarrow CH_3CHOH + H \rightarrow CH_3COH + 2H$. It is of interest how controllable factors may enhance or suppress these reaction pathways. Our recent work on the sum over histories representation (SOHR) of kinetics will prove to be useful as a means to assign unique quantitative probabilities for the contribution of various competing catalytic pathways. [59-64]

In this work we investigate the role of adsorbed water molecules on the chemistry of ethanol/Cu(111), and in particular the mechanism by which water may influence the selectivity of the process. Water is bound to Cu(111) by 0.18eV [29] and is known to possess a low barrier to molecular diffusion. On the other hand, the barrier to dissociation is relatively high at 1.01eV.

Thus, we expect that a substantial coverage of mobile and molecularly intact H_2O molecules can be obtained at sufficiently high reactor pressures. Water is obviously important as a feedstock in the ESR process. It is also a promoting species for ethanol decomposition. It has been shown that the inclusion of water in a reaction can increase production yields of H_2 or other desired products in various catalytic reactions.[30-33] It is also known to enhance diffusion of tightly bound species on metal surfaces which can have a noticeable impact on rate of bimolecular reactions.[34,35] Derivatives of water, such as OH and OOH, are found to decrease energetic barriers in both ethanol and methanol steam reforming reactions.[36-40] Recently calculations determined that H_2O is able to stabilize a number of adsorbates on metal catalysts.[41,42] This stabilization can push the steam reforming reactions forward to final products instead of by-products desorbing easily back into the gas phase. Water can be used as an effective hydrogen-transfer catalyst as a co-adsorbed species and can also stabilize transition states by hydrogen bonding with the molecule of interest, thus decreasing the reaction barrier.[43-45] When used as a hydrogen-transfer catalyst, water will hydrogen-bond with the surface species loosening the strength of the H-bond and allowing for a favorable energetic barrier to exchange the hydrogen with the surface.[46,47] It is clear, however, that a complete understanding of the details of the mechanism behind water catalysis has yet to be achieved.

Inspired by mechanistic studies of water catalysis in gas and cluster phase reactions,[48-51] we propose a process illustrated in Figure 2. In this double H-atom exchange reaction, water and the substrate form a ring-like transition state in which water accepts an H-atom from one part of the substrate while also transferring an H- atom to a different location. This sort of process has been shown to be of importance in, e.g. keto-enol reactions in the gas phase. In this work we consider two such processes involving intermediates of the ethanol mechanism, $CH_3CHOH+H_2O \rightarrow CH_3CH_2O+H_2O$ and $CH_3COH+H_2O \rightarrow CH_3CHO+H_2O$. In terms of the chemical pathways described above, the first reaction could have the effect of switching the route $CH_3CH_2OH \rightarrow CH_3CHOH + H \rightarrow CH_3COH + 2H$ to the route $CH_3CH_2OH \rightarrow CH_3CH_2O + H \rightarrow CH_3CHO + 2H$, hence promoting the production of acetaldehyde. Likewise, the second water catalyzed process could switch $CH_3CH_2OH \rightarrow CH_3CHOH + H \rightarrow CH_3COH + 2H \rightarrow CH_3CO + 3H$ to the acetaldehyde producing process $CH_3CH_2OH \rightarrow CH_3CHOH+H \rightarrow CH_3COH+2H \rightarrow CH_3CHO+2H$. To determine the influence of this pathway switching mechanism on the selectivity of the ESR process requires a determination of the rates of the elementary steps to determine the

reactive branching ratio. We shall investigate this issue using the DFT described below. The kinetics of the system will then be formulated using the SOHR method.

The remainder of this paper is organized as follows. In Section 2 we outline the kinetic methods that are employed. In 2.A the DFT methods are presented. In 2.B the transition state theory (TST) expressions used to compute the rate coefficients are described along with the SOHR approach for the probabilities of chemical pathways. In 2.C a sub-mechanism for the ethanol system is presented that approximates the decomposition kinetics of CH_3CH_2OH. A simple expression for the product selectivity of the mechanism is presented. In Section 3 we describe the results obtained. It is found that adsorbed water has a strong effect on the production of the acetaldehyde by-product. Section 4 presents a brief conclusion.

2. Theoretical Methods

A. Density Functional Theory Calculations

The energetic calculations are performed with periodic DFT using the Vienna ab initio Simulation Package (VASP).[52-55] Exchange-correlation energies were computed with Perdew-Burke-Ernzerhof (PBE)[56] functional and interactions between core and valence electrons were modeled with the projector augmented wave (PAW)[57,58] method. The plane-wave energy cutoff value was 400 eV. The Cu(111) surface is calculated with 3 slabs where the top slab is relaxed and the bottom two layers are fixed in their bulk geometries. A 3 x 3 x 1 mesh is used for all calculations. The lattice constant found for the Cu(111) surface is 3.64 Å and contains a vacuum spacing of 22 Å. When a 4 slab calculation is performed the vacuum spacing is 19 Å. The energetic differences between increasing the slab thickness from 3 to 4 slabs was minimal (so the calculated values presented are those from the 3 slab model. The surface calculations contain a (3x3) unit cell which gives a coverage of 1/9 ML for each species studied. In order to find the transition states a nudged elastic band (NEB) method is performed using the VTST package. The forces were converged to 0.01 eV $Å^{-1}$ and a self-consistent loop of 10^{-6} eV. The transition states were confirmed by normal mode analysis of the Hessian matrix with the finite difference approach. The adsorption energies of the adsorbates used in the pathway switching reactions with water are tabulated in the supporting information.

B. Rate coefficients, branching ratios, and pathway probabilities

The rate coefficients for unimolecular processes, such as the abstraction reactions S-H→S+H, can be written using statistical theory as

$$k(T) = \eta \frac{k_B T}{h} \frac{Q^{\ddagger}}{Q_{SH}} e^{-\triangle V/k_B T} \qquad (2.1)$$

where $Q^{\ddagger}$ and Q_{SH} are the vibrational partition functions of the transition state and reagent, respectively, ΔV is the zero point corrected barrier height, k_B is Boltzmann's constant, and h is Planck's constant. Additionally, we have included the numerical factor η which accounts for the degeneracy of the reaction path. For a bimolecular reaction, such as the double hydrogen energy process SH′+H_2O→SH+HOH′, we have

$$k(T) = \eta \frac{k_B T}{h} \frac{Q^{\ddagger}}{Q_{SH} Q_{H_2O}} e^{-\triangle V/k_B T} \qquad (2.2)$$

where the quantities are similarly defined in units of coverage. In the simplest approximation, we can estimate the prefactors in these expressions using the prescription $k(T) = Ae^{-\triangle V/k_B T}$ with A=10^{-13}/s. In a more elaborate analysis, the partitions functions can be evaluated using a normal mode analysis at the stationary points,

$$Q = \prod_{i=1}^{N} \frac{1}{1 - \exp(-\frac{h\nu_i}{k_B T})} \qquad (2.3)$$

where N is 3n (n is the number of atoms) for a reagent species and 3n-1 for a transition state and ν_i are the vibrational frequencies. In this analysis, the vibrational surface modes are ignored in the computation of the partition functions.

At a branching point of the chemical mechanism, a species A_i can react by several sink reactions leading to several distinct products. We denote the instantaneous rates of those competing processes as R^i_1, R^i_2, R^i_3, etc., which are related to coverages by

$$R_j^i = k_j(T)\theta_i \qquad for\ A_i \underset{k_j}{\rightarrow} Product_j \qquad (2.4)$$

for unimolecular sink reactions of A_i, i.e. $A_i \rightarrow Product_j$ and

$$R_j^i = k_j(T)\theta_i \cdot \theta_m \qquad for\ A_i + A_m \underset{k_j}{\rightarrow} Product_j \qquad (2.5)$$

for bimolecular reactions $A_i + A_m \rightarrow Product_j$. A key descriptor that quantifies a reaction network is the branching ratio for decay of a species A_i due to reaction j which we define as

$$\Gamma_j^i = \frac{R_j^i}{\sum_{j\prime}^{sinks} R_{j\prime}^i} \qquad (2.6)$$

which takes a constant value in steady state. When the co-reagent in the bimolecular process is water, then $R_j^i = k_j(T)\theta_i \cdot \theta_{H20}$ and the branching fraction is dependent on θ_{H20}.

To determine the quantitative contribution of a given chemical pathway in a large mechanism, we employ the Sum Over Histories Representation (SOHR) of chemical kinetics.[59-64] A chemical pathway is defined as a sequence of species and reactions that follow a tagged atom or moiety through all or part of a chemical network. The pathway probability is then uniquely defined by Monte Carlo integration of a Markov chain product of rates. While the formalism is valid for transient kinetics of general time-dependent problems, the application to steady state situations gives a simple and intuitive result. Namely, the cumulative probability of passage along a given reaction route "*k*" is equal to the product of branching ratios along that pathway, i.e.

$$P_k = \prod_m \Gamma_{m(k)}^{i(k)} \qquad (2.7)$$

where *i(k)* and *m(k)* label the species and reactions along the route *k*. In the case of steady state kinetics, the branching ratios are simply the quotients of reaction rates, i.e. eq. (2.6). The product selectivity is then simply the fraction of probability moving to the selected product. Thus, the selectivity for product F, i.e. S(F), is

$$S(F) = \frac{\sum_k^{Paths\ to\ F} P_k}{\sum_k^{All\ Paths} P_k} \qquad (2.8)$$

We apply this formalism by following a carbon atom from adsorption as EtOH to desorption as final product. In principle, there are an infinite number of contributing pathways allowed by the graph in both the numerator and denominator of eq. (2.8). However, in a previous[59] study of the

SOHR method for methanol decomposition ($CH_3OH \rightarrow 2H_2+CO$), it was found that a much simpler description is accurate. It was concluded that a forward only model of the enumeration of the chemical pathway correctly describes the chemistry. In this model, the backward H-atom recombination steps were assumed to be unimportant and those paths are omitted from the description. Thus, a very small number of pathways can be used to evaluate eq. (2.8).

C. Sub-mechanism

Within the large ethanol mechanism shown in Fig. 1, we identify a sub-mechanism responsible for the production of the acetaldehyde by-product that is highlighted using a dashed line. In the oval shaped region marked in Fig. 1, we see the initial reaction steps of an adsorbed EtOH molecule and the desorption of the acetaldehyde product. If the backward recombination reactions are neglected invoking the forward only-model, a followed carbon atom having once exited the sub-mechanism will not return. Instead, those carbon atoms continue on to form the products CH_4, CO, CO_2, CH_2O, $CH_3CH_2CH_3$, and $CH_3COOCH_2CH_3$. This is depicted in Fig. 3 where the reactions are numbered consistent with Table 1. As noted above, there are two direct pathways leading to $CH_3CHO(g)$ allowed by the forward only sub-mechanism: Pathway 1 (EtOH $\rightarrow$ CH_3CH_2O $\rightarrow$ CH_3CHO $\rightarrow$ $CH_3CHO(g)$) and Pathway 2 (EtOH $\rightarrow$ CH_3CHOH $\rightarrow$ CH_3CHO $\rightarrow$$CH_3CHO(g)$). These two paths are explicitly shown in Fig. 4 labeled by "1" and "2". Also shown in Fig. 4 are two water catalyzed pathways, labeled "3" and "4", that can lead to the acetaldehyde product as well.

Using the sub-mechanism and the SOHR method, the selectivity of $CH_3CHO(g)$ product formation is approximated using the sum of pathways leading to $CH_3CHO(g)$ based on the four critical juncture points A-D. These juncture points and the branching ratios are explicitly

A: $CH_3CH_2OH \rightarrow CH_3CH_2O+H$ (Γ_A^1) or $CH_3CHOH+H$(Γ_A^2)

B: $CH_3CHOH \rightarrow CH_3COH+H$ (Γ_B^1) , or CH_3CHO+H (Γ_B^2) , or $CH3CH_2O$ (Γ_B^3)

C: $CH_3COH \rightarrow CH_3CO+H$ (Γ_C^1) , or CH_3CO+H (Γ_C^2)

D: $CH_3CHO \rightarrow CH_3CHO(g)$ (Γ_D^1) , or CH_3CO+H (Γ_D^2)

From the sub-mechanism, it is clear that selectivity is given by

$$S(CH_3CHO) = \Gamma_A^1\Gamma_D^1 + \Gamma_A^2\Gamma_B^2\Gamma_D^1 + \Gamma_A^2\Gamma_B^3\Gamma_D^1 + \Gamma_A^2\Gamma_B^1\Gamma_C^2\Gamma_D^1 \qquad (2.9)$$

which correspond sequentially to the four paths shown in Fig. 4. The branching ratios at each node obviously add to unity and are independent of the species coverage although they do depend on coverage of H_2O.

3. Results and Discussion

The activation barriers for the reactions within the ethanol sub-mechanism for the Cu(111) surface have been obtained using DFT and are given in Table 1. We note that the hydrogen abstraction barriers have been computed previously by Zhang *et al.*[7,16] We call attention to several salient facts for the mechanism in the absence of adsorbed water. First, the barriers of the initial H-atom abstraction reactions $CH_3CH_2OH \rightarrow CH_3CHOH+H$ and $CH_3CH_2OH \rightarrow CH_3CH_2O+H$ are nearly equal, 1.02 eV vs 1.05 eV. This suggests a comparable fraction of the reactive flux will pass in both directions. We consider the kinetics at a reactor temperature of T=500K. At these conditions the branching ratios Γ_A^1 and Γ_A^2 are 0.33 and 0.67, respectively. Next, we note that desorption barrier for acetaldehyde ($CH_3CHO^* \rightarrow CH_3CHO(g)$) is substantially less than the reaction barrier $CH_3CHO \rightarrow CH_3CO+H$, 0.22eV vs 0.56eV. Thus, we predict that the vast majority of molecules arriving at CH_3CHO^* will in fact desorb into the gas phase, i.e. $\Gamma_D^1 \approx 1$. The third important branching point of the sub-mechanism is the reaction $CH_3CHOH \rightarrow CH_3COH+H$ (or $\rightarrow CH_3CHO+H$). We find the energetics favors the CH_3COH pathway 0.53 eV vs 0.70 eV. Thus, theory suggests that probabilities for the two $CH_3CHO(g)$ forming processes shown in Fig. 4 should be quite substantial on this surface. On a dry surface at 500K we estimate the selectivity is $S(CH_3CHO)=0.345$ based on the energetics.

In addition to activation energies, there are also entropic factors that enter into the rate coefficients through the vibrational frequencies. We have computed the frequencies for a number of the abstraction reactions and have found that they do not greatly alter the simple prescription $A=10^{13}/s$ which we shall use in our numerical estimates of the pathway probabilities.

In order to examine the influence of the water catalyzed reactions on the selectivity of acetaldehyde production, we have also computed the transition state structures and energetics for the two water catalyzed reactions indicated shown with dashed lines in Fig. 3. Consider first the process $CH_3CHOH'+HOH'' \rightarrow$ and $CH_3CHH''O+HOH'$, which facilitates the production of acetaldehyde via pathway 3. We add distinguishing primes to the H-atoms to clarify the

mechanism. This double H-atom exchange reaction requires the donor alcohol H′-atom transfer to occur in concert with the acceptance of an H″-atom from water. The barrier energy for this reaction is found to be E_a=0.45eV and the exothermicity is ΔE_{rxn}=-0.81eV. The formation of the transition state structure obtained using the NEB image climbing method is shown in Fig. 5 where we have colored the exchanging H-atoms for clarity. Formation of the transition state (TS) requires the H_2O species to undergo a large amplitude displacement and, simultaneously, the OH-group of CH_3CHOH reorients towards H_2O. The TS forms a puckered 5-member ring-like structure similar to analogous gas phase reactions. However, the water molecule remains relatively further apart from CH_3CHOH for the surface reaction compared with the gas phase. Binding to the Cu surface clearly provides substantial stabilization of the TS. We also note the ethanol derivative significantly displaces during the reaction as the reagent CH_3CHOH is bound to the surface through the middle carbon atom at a top site while product CH_3CH_2O is bound through the oxygen atom on a 3-fold site. The second process, $CH_3COH'+HOH''\rightarrow CH_3CH''O+HOH'$, is also a donor-acceptor double exchange reaction. Three structures along the reaction path are shown in Fig. 6 with the middle image corresponding to the TS. While there are similarities to the previous reaction, it is seen that the reagent species, here CH_3COH, undergoes a much more significant reorientation than for the previous reaction. The relative orientation of the reagent species at the TS is clearly quite distinct from that the first reaction. The CH_3COH is bound to the surface through the middle carbon atom on a top site and CH_3CHO is bound to the surface through the oxygen atom. The barrier energy for this reaction is low, E_a=0.16eV, with an exothermicity of ΔE_{rxn}= -0.48eV. The potential role of entropic factors in the rate expression was also of some concern for these reactions. However, our estimates of the vibrational frequencies again lead to the conclusion that simple choice $A=10^{13}$/s was accurate to within about a factor of 2 for T=500K.

To access how the water catalyzed reactions might compete with the conventional abstraction reactions, we have plotted the reaction energetics for the chemistry emanating from the CH_3CHOH and CH_3COH species in Figs. 7 and 8, respectively. The energies of the reactants containing water have an initial energy of -0.18 eV due to the adsorption energy of water. The CH_3CHOH moiety can react in three ways, to form CH_3COH, CH_3CHO, or (via water catalysis) CH_3CH_2O. As seen in Fig. 7, in the absence of surface water the CH_3COH channel is favored with the lowest barrier of 0.53eV. Reactions following this branch go on to form products that avoid the CH_3CHO(g) by-product. However, when water is present, the CH_3CH_2O channel is favored with the lower barrier

of 0.45eV. This water catalyzed process thus enhances the production of $CH_3CHO(g)$ via pathway 3. In Fig. 8 we show the possible reactions of CH_3COH, i.e. $CH_3COH \rightarrow CH3CO+H$ and $CH_3COH+H_2O \rightarrow CH_3CHO+H_2O$. It is seen that the barrier to the water catalyzed process is a factor of two lower than that of the abstraction reaction, i.e. 0.16eV versus 0.32 eV. This suggests that a significant shift in the product selectivity may be induced by water at this juncture point in the mechanism via pathway 4.

Since the water catalyzed reactions are nominally 2^{nd}-order bimolecular processes, the reaction rates depend on level of H_2O coverage, θ_{H2O}. This naturally leads to a similar dependence of the branching ratios and product selectivity. The value of θ_{H2O} can be viewed as a control parameter that can varied using the reactor conditions, such as pressure and mole fraction of feed gas. Some representative results at T=500K have been computed for four values of θ_{H2O} , 0, 0.001ML, 0.01ML, and 0.05ML. The coverage of ethanol and its derivatives are assumed to be small and do not affect the numerical results. In Fig. 9, we show the sensitivity of the pathway probabilities and the product selectivity as this parameter is varied. The explicit values are shown for the probabilities P_1-P_4 of the four $CH_3CHO(g)$ producing paths along with the resulting product selectivity, $S(CH_3CHO)$. To aid in the visualization, the CH_3CHO producing routes are shown in their respective colors from Fig. 4 and desorption of CH_3CHO is gray while the flux proceeding to other products is in green. The thickness of the lines reflects the magnitude of the flux and the use of dashed lines indicates pathway switching routes catalyzed by the surface water. In panel A, $\theta_{H2O}=0$, the reaction largely avoids the $CH_3CHO(g)$ by-product by proceeding along the route $CH_3CH_2OH \rightarrow CH_3CHOH \rightarrow CH_3COH \rightarrow CH_3CO \rightarrow$product. The selectivity is $S(CH_3CHO)=0.345$. As the water coverage is increased, the contribution from the catalyzed pathways 3 and 4 begin to contribute. By the point where the surface coverage has risen to $\theta_{H2O}=0.05$, we see that $P_3=0.160$ and $P_4=0.335$. At this high level of surface water, the probabilities of catalyzed reaction pathways have actually surpassed those of the direct pathways, 1 and 2. The product selectivity has dramatically increased to $S(CH_3CHO)=0.836$ by the point $\theta_{H2O}=0.05$. We note that even at very low levels of water coverage the product selectivity is measurably affected by the catalyzed pathways, i.e. $S(CH_3CHO)=0.375$ at $\theta_{H2O}=0.001$ versus 0.345 at $\theta_{H2O}=0$.

The role of surface water in modifying the product branching is quantitatively understood from Fig. 9. At the branching point "B", corresponding to the intermediate CH_3CHOH, the

fraction of flux going to $CH_3CHO(g)$ product grows from $\Gamma_B^2 + \Gamma_B^3 = 0.02$ at θ_{H2O} =0 to $\Gamma_B^2 + \Gamma_B^3 = 0.25$ at θ_{H2O} =0.05. Even more significantly, at the branching point "C", the fraction of flux going to $CH_3CHO(g)$ product grows from $\Gamma_C^2 = 0$ at θ_{H2O} =0 to $\Gamma_C^2 = 0.67$ at θ_{H2O} =0.05. Surface water thus reroutes the reaction flux in the network by a factor of 2.4 suggesting that water coverage may be an effective control parameter for surface selectivity.

4. Conclusion

The kinetics of the key reaction steps in the ethanol decomposition chemistry on Cu(111) are computed using a combination of the DFT theory and statistical rate theory. The global transport of flux in the chemical network is analyzed using the SOHR method. The product selectivity for the formation of the acetaldehyde by-product under steady state condition is formulated in terms of the branching probabilities at four key juncture points in the reaction network.

The main focus of this work was to investigate the influence of adsorbed molecular water as a catalyst in the decomposition kinetics of ethanol. Two water catalytic reactions were explored, i.e. $CH_3CHOH+H_2O \rightarrow CH_3CH_2O+H_2O$ and $CH_3COH+H_2O \rightarrow CH_3CHO+H_2O$. These are double H-atom exchange reactions where an H-atom removed from one part the of a species and reattached at a different location. Since the process has some concerted character, the barrier is lower than that predicted from two sequential reaction steps. It was found that adsorbed water gave rise to a pathway shifting effect in which reactive flux is re-routed on the surface to favor $CH_3CHO(g)$ by-product. This increase in acetaldehyde productison aligns with catalyst sensitivity from experimental work. The surface coverage of H_2O can be viewed as a control parameter that can be used to adjust the product yield. It was found in the present case of low coverage Cu(111)/EtOH that product yield for acetaldehyde can be increased by a factor of 2.4 by a water coverage of θ_{H2O}=0.05ML. While further calculations with functionals that describe vdW interactions with higher accuracy, such as the BEEF-vdW functional[65], would lead to more accurate energetic barriers the results presented here are a good first step towards examining these bimolecular reactions with water.

It is clear that adsorbed water can influence the chemistry of catalyzed decomposition reactions in a variety of ways. Since water is almost always present at some level in realistic reaction

environments it is important to understand the principles that govern this sensitivity. There are two levels of analysis that we might employ to investigate these effects: (1) how water promotes or inhibits the rates of individual elementary reactions through, e.g., stabilizing the TS, or (2) how water modifies the global reactive flux of the chemical network. Although these approaches are obviously linked, we suggest the latter avenue may be the more generally useful. An individual reaction step may be highly catalyzed by surface water but still have no influence on observables if it is not a key rate limiting process. In this work we have emphasized the role of water at key juncture points in the network as a means of controlling the global reaction pathways. In the present case we demonstrated that this viewpoint yields a clear understanding of aspects of product selectivity.

ASSOCIATED CONTENT

Supporting Information

Included are the VASP Poscar coordinates of the initial state, transition state, and final state of the two bimolecular reactions that include water. In addition to the Poscar coordinates, the vibrational frequencies of each transition state as well as the calculated adsorbate energies of all atoms involved in these reactions are presented. This material is available free of charge via the Internet at http://pubs.acs.org.

AUTHOR INFORMATION

Corresponding Author

* rex.skodje@colorado.edu

Notes

The authors declare no competing financial interests.

Acknowledgements

This work was supported by the National Science Foundation through grant CHE1556041. This work utilized the RMACC Summit supercomputer, which is supported by the National Science Foundation (awards ACI-1532235 and ACI-1532236), the University of Colorado Boulder, and Colorado State University. The Summit supercomputer is a joint effort of the University of Colorado Boulder and Colorado State University.

References

[1] Somorjai, G. A.; Li, Y. *Introduction to Surface Chemistry and Catalysis*; John Wiley & Sons: Hoboken NJ, **2010**.
[2] Hammer, B.; Nørskov, J. K. Theoretical Surface Science and Catalysis – Calculations and Concepts. *Adv. Catal.* **2000**, *45*, 71-129.
[3] Nørskov, J. K.; Abild-Pedersen, F.; Studt, F.; Bligaard, T. Density Functional Theory in Surface Chemistry and Catalysis. *Proc. Natl. Acad. Sci.* **2011,** *108*, 937-943.
[4] Ferrin, P.; Simonetti, D.; Kandoi, S.; Kunkes, E.; Dumesic, J. A.; Nørskov, J. K.; Mavrikakis, M. Modeling Ethanol Decomposition on Transition Metals: A Combined Application of Scaling and Brønsted-Evans-Polanyi Relations. *J. Am. Chem. Soc.* **2009**, *131*, 5809-5815.
[5] Wang, H.F.; Liu, Z.P. Comprehensive Mechanism and Structure-Sensitivity of Ethanol Oxidation on Platinum: New Transition-State Searching Method for Resolving the Complex Reaction Network. *J. Am. Chem. Soc.* **2008**, *130*, 10996-11004.
[6] Wang, J.; Zhang, X.; Sun, Q.; Chan, S.; Su, H. Chain Growth Mechanism on Bimetallic Surfaces for Higher Alcohol Synthesis from Syngas. *Catal. Commun.* **2015**, *61,* 57-61.
[7] Zhang, R.; Wang, G; Wang, B. Insights into the Mechanism of Ethanol Formation from Syngas on Cu and an Expanded Prediction of Improved Cu-Based Catalyst. *J. Catal.* **2013**, *305*, 238–255.
[8] Zanchet, D.; Santos, J. B. O.; Damyanova, S.; Gallo, J. M. R.; Bueno, J. M. C. Toward Understanding Metal-Catalyzed Ethanol Reforming. *ACS Catalysis* **2015**, *5*, 3841-3863.
[9] Yang, Y.; White, M. G.; Liu, P. Theoretical Study of Methanol Synthesis from CO2 Hydrogenation on Metal-Doped Cu(111) Surfaces. *J. Phys. Chem. C* **2011**, *116*, 248-256.
[10] Navarro, R. M.; Pena, M. A.; Fierro, J. L. G. Hydrogen Production Reactions from Carbon Feedstocks: Fossil Fuels and Biomass. *Chem. Rev.* **2007**, *107*, 3952−3991.
[11] Wang, S. S.; Gu, X. K.; Su, H. Y.; Li, W. X. First-Principles and Microkinetic Simulation Studies of the Structure Sensitivity of Cu Catalyst for Methanol Steam Reforming. *J. Phys. Chem. C* **2018**, *122*, 10811−10819.
[12] Wang, S. S.; Su, H. Y.; Gu, X. K.; Li, W. X. Differentiating Intrinsic Reactivity of Copper, Copper−Zinc Alloy, and Copper/Zinc Oxide Interface for Methanol Steam Reforming by First-Principles Theory. *J. Phys. Chem. C* **2017**, *121*, 21553−21559.
[13] Zheng, H.; Zhang, R.; Li, Z.; Wang, B. Insight into the Mechanism and Possibility of Ethanol Formation from Syngas on Cu(100) Surface, *J. Mol. Catal.* **2015**, *404–405*, 115–130.
[14] Sutton, J. E.; Panagiotopoulou, P.; Verykios, X. E.; Vlachos, D. G. Combined DFT, Microkinetic, and Experimental Study of Ethanol Steam Reforming on Pt. *J. Phys. Chem. C* **2013**, *117*, 4691-4706.
[15] Li, R.; Zhang, M.; Yu, Y. A DFT Study on the Cu (111) Surface for Ethyl Acetate Synthesis from Ethanol Dehydrogenation. *Appl. Surf. Sci.* **2012**, *258*, 6777–6784.

[16] Zhang, M.; Yao, R.; Jiang, H.; Li, G.; Chen, Y. Catalytic Activity of Transition Metal Doped Cu(111) Surfaces for Ethanol Synthesis from Acetic Acid Hydrogenation: a DFT Study. *RSC Adv.* **2017**, 7, 1443-1452.
[17] Xiang, N.; Xu, P.; Ran, N.; Ye, T. Production of Acetic Acid from Ethanol over CuCr Catalysts *via* Dehydrogenation-(Aldehyde-Water Shift) Reaction. *RSC Adv.* **2017**, *7*, 38586-38593.
[18] Alcala, R.; Mavrikakis, M.; Dumesic, J. A. DFT Studies for Cleavage of C-C and C-O Bonds in Surface Species Derived from Ethanol on Pt(111). *J. Catal.* **2003**, *218*, 178-190.
[19] Li, H.; Evans Jr., E. J.; Mullins, C. B.; Henkelman, G. Ethanol Decomposition on Pd–Au Alloy Catalysts. *J. Phys. Chem. C* **2018,** *122*, 22024-22032.
[20] Li, H.; Henkelman, G. Dehydrogenation Selectivity of Ethanol on Close-Packed Transition Metal Surfaces: A Computational Study of Monometallic, Pd/Au, and Rh/Au Catalysts. *J. Phys. Chem. C* **2017**, *121*, 27504-27510.
[21] Sun, K.; Zhang, M.; Wang, L. Effects of Catalyst Surface and Hydrogen Bond on Ethanol Dehydrogenation to Ethoxy on Cu Catalysts. *Chem. Phys. Lett.* **2013**, *585*, 89–94.
[22] Wu, R.; Wang, L. Alloying Effect via Comparative Studies of Ethanol Dehydrogenation on Cu(111), Cu_3Pd(111), and Cu_3Pt(111). *Chem. Phys. Let.* **2017**, *678*, 196–202.
[23] Wang, Z. T.; Xu, Y.; El-Soda, M.; Lucci, F. R.; Madix, R. J.; Friend, C. M.; Sykes, E. C. H. Surface Structure Dependence of the Dry Dehydrogenation of Alcohols on Cu(111) and Cu(110). *J. Phys. Chem. C* **2017** *121*, 12800-12806.
[24] Li, F.; Jiang, D. E.; Zeng, X. C.; Chen, Z. Mn Monolayer Modified Rh for Syngas-to-Ethanol Conversion: A First-Principles Study, *Nanoscale* **2012**, *4*, 1123-1129.
[25] Sun, X.; Zhang, R.; Wang, B. Insights into the Preference of CHx(x=1–3) Formation from CO Hydrogenation on Cu(111) Surface. *Appl. Surf. Sci.* **2013**, *265*, 720-730.
[26] Kumar, A.; Mukasyan, A.S.; Wolf, E.E. Combustion Synthesis of Ni, Fe and Cu Multi-Component Catalysts for Hydrogen Production from Ethanol Reforming. *Applied Catal. A* **2011**, *401*, 20-28.
[27] Marino, F.; Boveri, M.; Baronetti, G.; Laborde, M. Hydrogen Production via Catalytic Gasification of Ethanol. A Mechanism Proposal over Copper–Nickel Catalysts. *Int. J. Hydrogen Energ.* **2004**, *29*, 67-71.
[28] Velu, S.; Satoh, N.; Gopinath, C.S.; Suzuki, K. Oxidative Reforming of Bio-Ethanol over CuNiZnAl Mixed Oxide Catalysts for Hydrogen Production. *Catal. Lett.* **2002**, *82*, 145-152.
[29] Prats, H.; Alvarez, L.; Illas, F.; Sayos, R. Kinetic Monte Carlo Simulations of the Water Gas Shift Reaction on Cu(111) from Density Functional Theory Based Calculations. *J. Catal.* **2016**, *333*, 217-226.
[30] Chang, C.R.; Huang Z.Q.; Li, J. The Promotional Role of Water in Heterogeneous Catalysis: Mechanism Insights from Computational Modeling. *Wiley Interdiscip. Rev. Comput. Mol. Sci.* **2016**, *6*, 679–93.
[31] Boucher, M. B.; Marcinkowski, M. D.; Liriano, M. L.; Murphy, C. J.; Lewis, E. A.; Jewell, A. D.; Mattera, M. F. G.; Kyriakou, G.; Flytzani-Stephanopoulos, M.; Sykes, E. C. H. Molecular-Scale Perspective of Water-Catalyzed Methanol Dehydrogenation to Formaldehyde. *ACS Nano* **2013**, *7*, 6181−6187.
[32] Chibani, S.; Michel, C.; Delbecq, F.; Pinel, C.; Besson, M. On the Key Role of Hydroxyl Groups in Platinum-Catalysed Alcohol Oxidation in Aqueous Medium. *Catal. Sci. Technol.* **2013**, *3*, 339–350.
[33] Saavedra, J.; Doan, H.A.; Pursell, C.J.; Grabow, L.C.; Chandler, B.D. The Critical Role of Water at the Gold-Titania Interface in Catalytic CO Oxidation. *Science* **2014**, *345*, 1599–1602.
[34] Xu, F.; Fampiou, I.; O'Connor, C.R.; S. Karakalos, S.; Hiebel, F.; Kaxiras, E.; Madix, R.J.; Friend, C. Water Facilitates Oxygen Migration on Gold Surfaces. *Phys. Chem. Chem. Phys.* **2018**, *20*, 2196-2204.
[35] Merte, L.R.; Peng, G.; Bechstein, R.; Rieboldt, F.; Farberow, C.A.; Grabow, L.C.; Kudernatsch, W.; Wendt, S.; Lægsgaard, E.; Mavrikakis, M.; Besenbacher, F. Water-Mediated Proton Hopping on an Iron Oxide surface. *Science*, **2012**, *336*, 889-893.
[36] Chang, C. R.; Yang, X.F.; Long, B.; Li J. A Water-Promoted Mechanism of Alcohol Oxidation on a Au(111) Surface: Understanding the Catalytic Behavior of Bulk Gold. *ACS Catal.* **2013**, *3*, 1693-1699.
[37] Chang, C.R.; Wang, Y.G.; Li, J. Theoretical Investigations of the Catalytic Role of Water in Propene Epoxidation on Gold Nanoclusters: A Hydroperoxyl-Mediated Pathway. *Nano Res.* **2011**, *4*, 131–142.

[38] Sheu, W.S.; Chang, M.W. CO Oxidation on Ag(111): The Catalytic Role of H_2O. *Surf. Sci.* **2014**, *628*, 104-110.
[39] Ran, Y.X.; Du, Z.Y.; Guo, Y.P.; Feng, J.; Li, W.Y. Density Functional Theory Study of Acetic Acid Steam Reforming on Ni(111). *Appl. Surf. Sci.* **2017**, *400*, 97-109.
[40] Xu, D.; Wu, P.; Yang, Bo. Essential Role of Water in the Autocatalysis Behavior of Methanol Synthesis from CO2 Hydrogenation on Cu: A Combined DFT and Microkinetic Modeling Study *J. Phys. Chem. C* **2019**, *123*, 8959-8966.
[41] Miller, K.L.; Musgrave, C.B.; Falconer, J.L.; Medlin, J.W. Effects of Water and Formic Acid Adsorption on the Electronic Structure of Anatase TiO_2(101). *J Phys. Chem. C* **2011**, *115*, 2738-2749.
[42] Su, H.Y.; Yang, M.M.; Bao, X.H.; Li, W.X. The Effect of Water on the CO Oxidation on Ag(111) and Au(111) Surfaces: A First-Principle Study. *J. Phys. Chem. C* **2008**, *112*, 17303-17310.
[43] Zhao, Y.F.; Yang, Y.; Mims, C.; Peden, C.H.F.; Li, J. Mei, D. Insight into Methanol Synthesis from CO_2 Hydrogenation on Cu(111): Complex Reaction Network and the Effects of H_2O, *J. Catal.* **2011**, *281*, 199-211.
[44] Zaffran, J.; Michel, C.; Delbecq, F.; Sautet, P. Towards More Accurate Prediction of Activation Energies for Polyalcohol Dehydrogenation on Transition Metal Catalysts in Water. *Catal. Sci. Technol.* **2016**, *6*, 6615-6624.
[45] Nie, X.; Jiang, X.; Wang, H.; Luo, W.; Janik, J.J.; Chen, Y.; Guo, X.; Song, C. Mechanistic Understanding of Alloy Effect and Water Promotion for Pd-Cu Bimetallic Catalysts in CO_2 Hydrogenation to Methanol. *ACS Catalysis* **2018,** *8*, 4873-4892.
[46] Huang, Z.Q.; Long, B.; Chang, C.R. A Theoretical Study on the Catalytic Role of Water in Methanol Steam Reforming on PdZn(111). *Catal. Sci. Technol.* **2015**, *5*, 2935-2944.
[47] Du, Z.Y.; Ran, Y.X.; Guo, Y.P.; Feng, J.; Li, W.Y. A Theoretical Study on the Role of Water and its Derivatives in Acetic Acid Steam Reforming on Ni(111). *Appl. Surf. Sci.* **2017**, *419*, 114-125.
[48] Morokuma, K.; Muguruma, C. Ab Initio Molecular Orbital Study of the Mechanism of the Gas Phase Reaction $SO_3 + H_2O$: Importance of the Second Water Molecule. *J. Am. Chem. Soc.* **1994**, *116*, 10316-10317.
[49] Aloisio, S.; Francisco, J.S. Radical-Water Complexes in Earth's Atmosphere. *Acc. Chem. Res.* **2000**, *33*, 825-830.
[50] Takahashi, K.; Kramer, Z.C.; Vaida, V.; Skodje, R.T. Vibrational Overtone Induced Elimination Reaction Within Hydrogen-Bonded Molecular Clusters: The Dynamics of Water Catalyzed Reactions in $CH_2FOH\ (H_2O)_n$. *Phys. Chem. Chem. Phys.* **2007**, *9*, 3864-3871.
[51] Kramer, Z.C.; Takahashi, K.; Skodje, R.T. Water Catalysis and Anticatalysis in Photochemical Reactions: Observation of a Delayed Threshold Effect in the Reaction Quantum Yield. *J. Am. Chem. Soc.* **2010**, *132*, 15154-15157.
[52] Kresse, G.; Hafner, J. Ab Initio Molecular Dynamics for Liquid Metals. *Phys. Rev. B: Condens. Matter Mater. Phys.* **1993**, *47*, 558-561.
[53] Kresse, G.; Hafner, J. Ab Initio Molecular-Dynamics Simulation of the Liquid-Metal-Amorphous Semiconductor Transition in Germanium. *Phys. Rev. B: Condens. Matter Mater. Phys.* **1994**, *49*, 14251-14269.
[54] Kresse, G.; Furthmüller, J. Efficiency of Ab-Initio Total Energy Calculations for Metals and Semiconductors Using a Plane-wave Basis Set. *Comput. Mater. Sci.* **1996**, *6*, 15-50.
[55] Kresse, G.; Furthmuller, J. Efficient Iterative Schemes for Ab Initio Total-energy Calculations Using a Plane-wave Basis Set. *Phys. Rev. B: Condens. Matter Mater. Phys.* **1996**, *54*, 11169−11186.
[56] Perdew, J. P.; Burke, K.; Ernzerhof, M. Generalized Gradient Approximation Made Simple. *Phys. Rev. Lett.* **1996**, *77*, 3865-3868.
[57] Blöchl, P. E. Projector Augmented-wave Method. *Phys. Rev. B: Condens. Matter Mater. Phys.* **1994**, *50*, 17953-17979.
[58] Kresse, G.; Joubert, D. From Ultrasoft Pseudopotentials to the Projector Augmented-Wave Method. *Phys. Rev. B: Condens. Matter Mater. Phys.* **1999**, *59*, 1758-1775.
[59] Wells, R.H.; Gu, X.K.; Li, W.X.; Skodje, R.T. *J. Phys. Chem. C* **2018** *122*, 28158-28172.

[60] Bai, S.; Skodje, R. T. Simulating Chemical Kinetics Without Differential Equations: A Quantitative Theory Based on Chemical Pathways. *J. Phys. Chem. Lett.* **2017**, *8*, 3826-3833.
[61] Bai, S. R.; Skodje, R. T. The Sum Over Histories Representation for Chemical Kinetics: A Quantitative Theory Based on Chemical Pathways. *Int. Rev. Phys. Chem.* **2016**, *35*, 539-567.
[62] Bai, S. R.; Zhou, D. Y.; Davis, M. J.; Skodje, R. T. Sum Over Histories Representation for Chemical Kinetics. *J. Phys. Chem. Lett.* **2015**, *6*, 183-188.
[63] Bai, S. R.; Davis, M. J.; Skodje, R. T. Sum over Histories Representation for Kinetic Sensitivity Analysis: How Chemical Pathways Change When Reaction Rate Coefficients Are Varied. *J. Phys. Chem. A* **2015**, *119*, 11039-11052.
[64] Bai, S.R.; Sivaramakrishnan, R.; Davis, M.J.; Skodje, R.T. A Chemical Pathway Perspective on Low Temperature Ignition of Propane. *Combust. and Flame* **2019**, *202*, 154-178.
[65] Wellendorff, J.; Lundgaard, K. T.; Mogelhoj, A.; Petzold, V.; Landis, D. D.; Norskov, J. K.; Bligaard, T.; Jacobsen, K. W. Density Functionals for Surface Science: Exchange-Correlation Model Development with Bayesian Error Estimation. *Phys. Rev. B* **2012**, *85*, 235149.

Elementary Step	E_a	ΔE_{rxn}
Dry Reactions		
1. $CH_3CH_2OH^* + * \rightarrow CH_3CHOH^* + H^*$	1.02	0.76
2. $CH_3CH_2OH^* + * \rightarrow CH_3CH_2O^* + H^*$	1.05	-0.05
3. $CH_3CHOH^* + * \rightarrow CH_3CHO^* + H^*$	0.70	-0.35
4. $CH_3CHOH^* + * \rightarrow CH_3COH^* + H^*$	0.53	0.13
5. $CH_3CH_2O^* + * \rightarrow CH_3CHO^* + H^*$	0.61	0.46
6. $CH_3CHO^* \rightarrow CH_3CHO(g) + *$	0.22	0.22
7. $CH_3CHO^* + * \rightarrow CH_3CO^* + H^*$	0.56	0.07
8. $CH_3COH^* + * \rightarrow CH_3CO^* + H^*$	0.32	-0.41
Wet Reactions		
9. $CH_3CHOH^* + H_2O^* \rightarrow CH_3CH_2O^* + H_2O^*$	0.45	-0.81
10. $CH_3COH^* + H_2O^* \rightarrow CH_3CHO^* + H_2O^*$	0.16	-0.48

Table 1: Barrier energies (in eV) for the reactions in the micro-kinetic model. Reactions 1-8 are the dry reactions (no water) while reactions 9-10 are the newly added wet reactions. E_a is the classical barrier energy and ΔE_{rxn} is the reaction energy of the individual reaction steps.

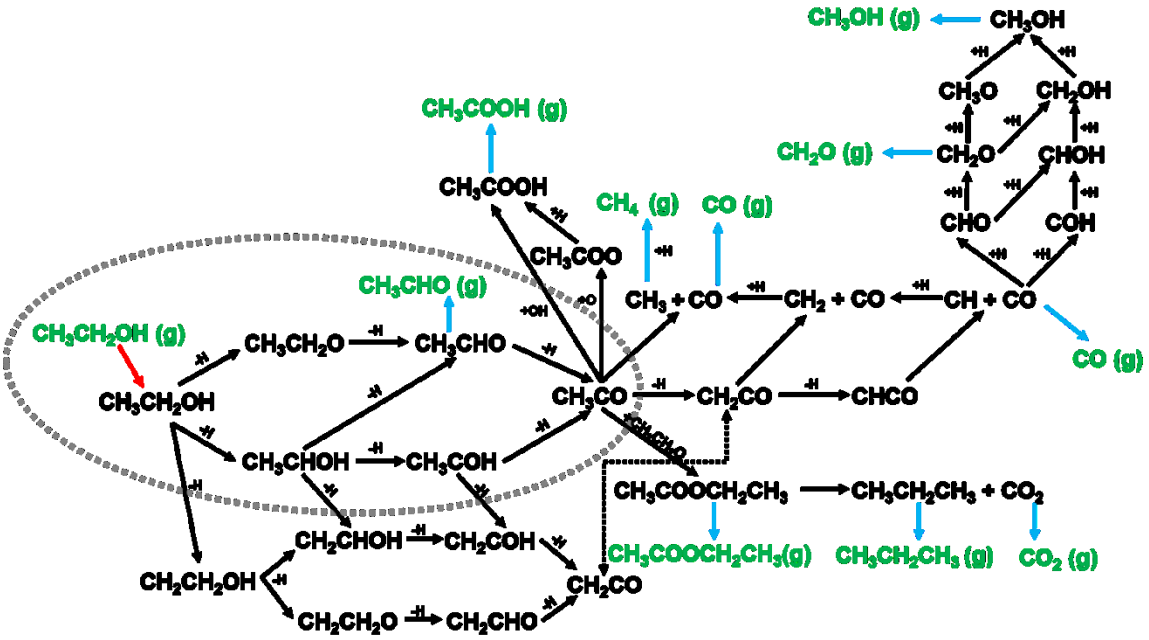

Figure 1: Mechanism for ESR reaction and related reactions from ethanol. The encircled portion of the mechanism contains the acetaldehyde production pathways. An initial EtOH molecule reaching CH_3CO will continue on towards the products CH_4, CO, CO_2, CH_2O, $CH_3CH_2CH_3$, and $CH_3COOCH_2CH_3$.

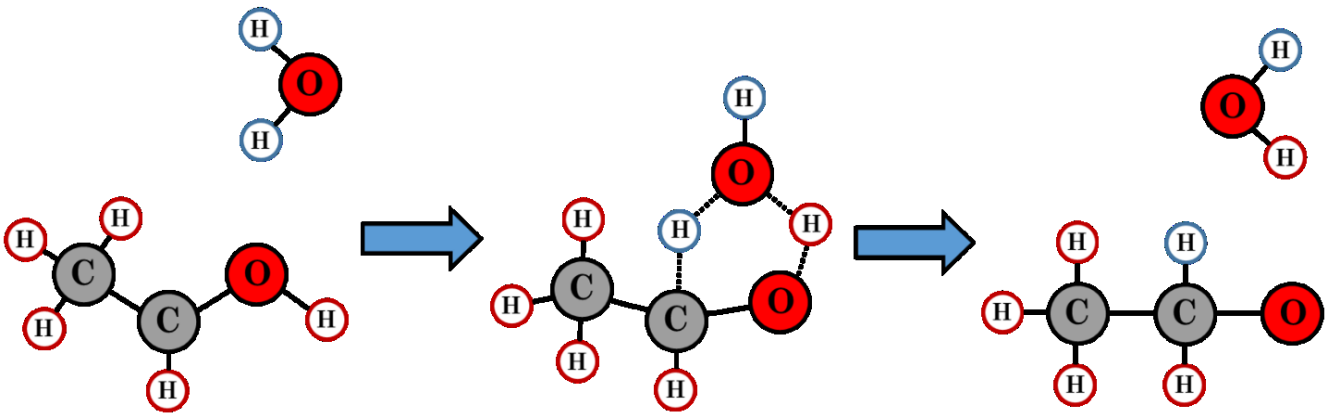

Figure 2: Proposed mechanism for pathway switching catalyzed by H_2O. In this mechanism, water accepts a hydrogen from the OH group of the substrate and donates a hydrogen to another atom on the substrate. While this reaction step does not further the decomposition process it switches the reaction route.

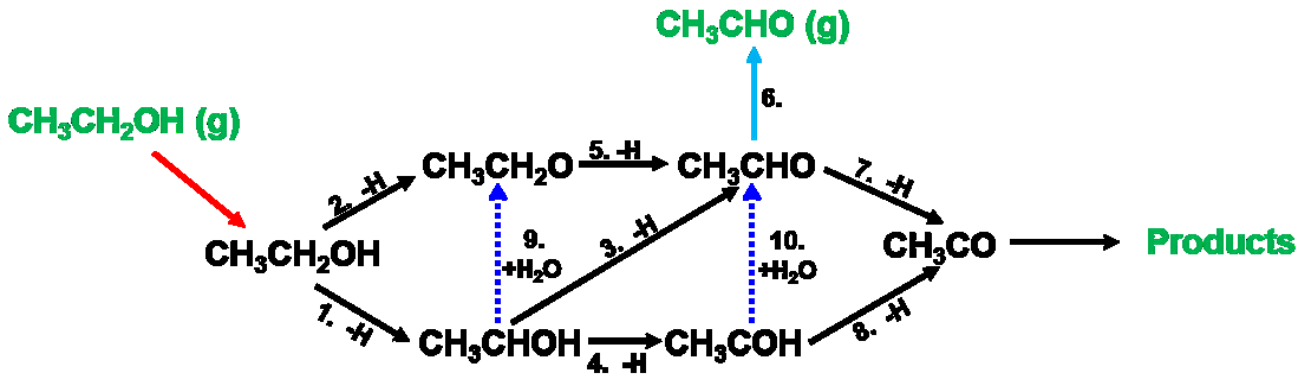

Figure 3: Network of ethanol decomposition to acetaldehyde or further products. Reactions 1-5,7, and 8 are hydrogen abstraction reactions. Reaction 6 is desorption of acetaldehyde into the gas phase. Reactions 9 and 10 are the newly added water pathway switching reactions.

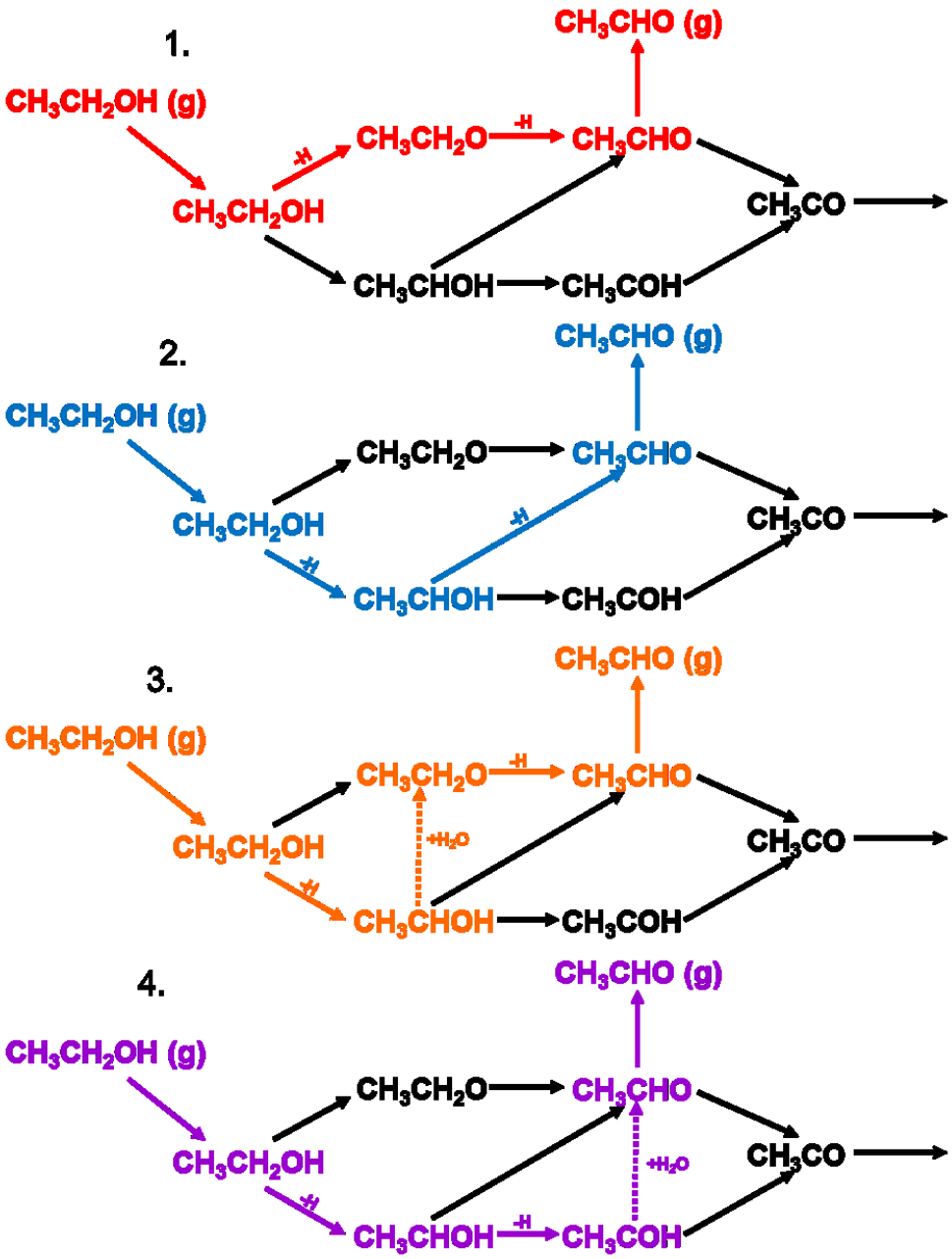

Figure 4: Chemical pathways from EtOH leading to $CH_3CHO(g)$. Pathways 1 and 2 include only H-abstraction reactions while pathways 3 and 4 also employ water catalyzed pathway switching reactions.

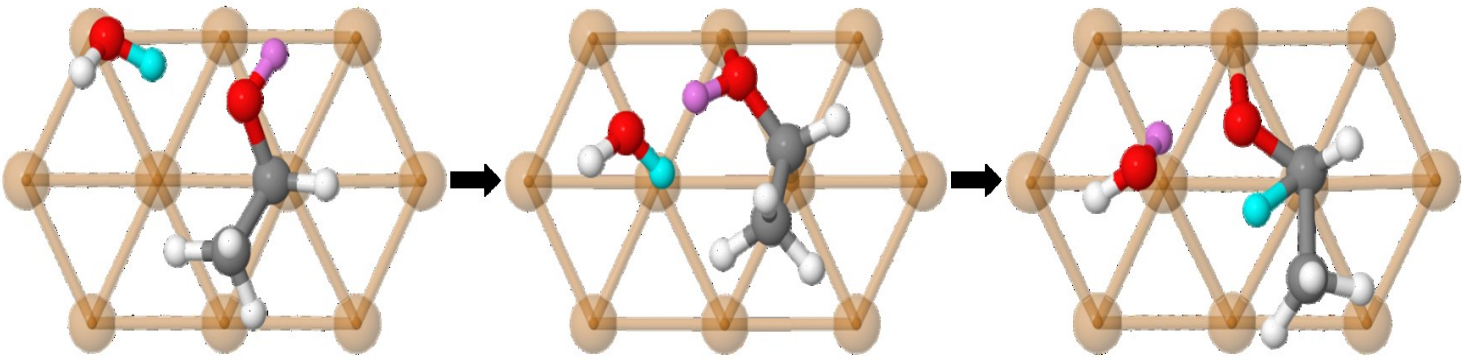

Figure 5: Configurations along the reaction path for $CH_3CHOH + H_2O \rightarrow CH_3CH_2O + H_2O$. The H_2O and EtOH derivative are seen to undergo large amplitude displacement prior to H-atom transfer. The (purple) OH-group reorients during the reaction. The middle image corresponds to the transition state.

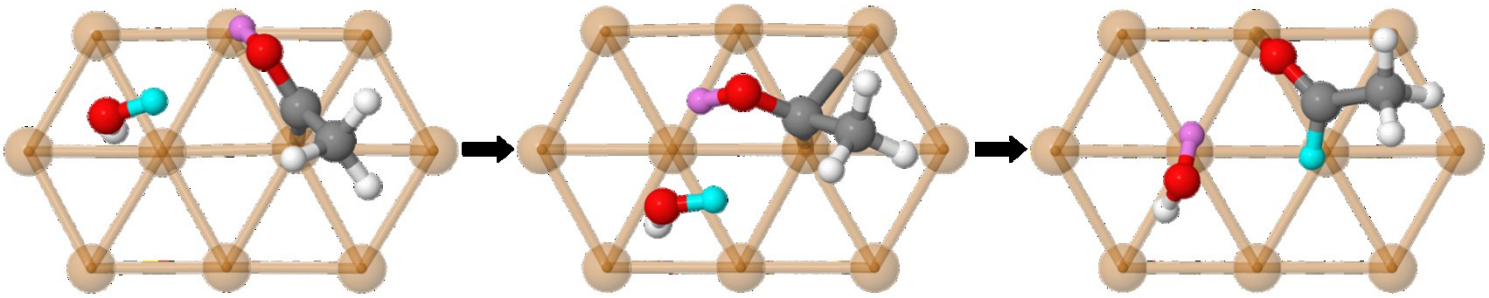

Figure 6: Configurations along the reaction path for $CH_3COH + H_2O \rightarrow CH_3CHO + H_2O$. The H_2O and the EtOH undergo large amplitude displacement during the course of the reaction. The middle image corresponds to the transition state.

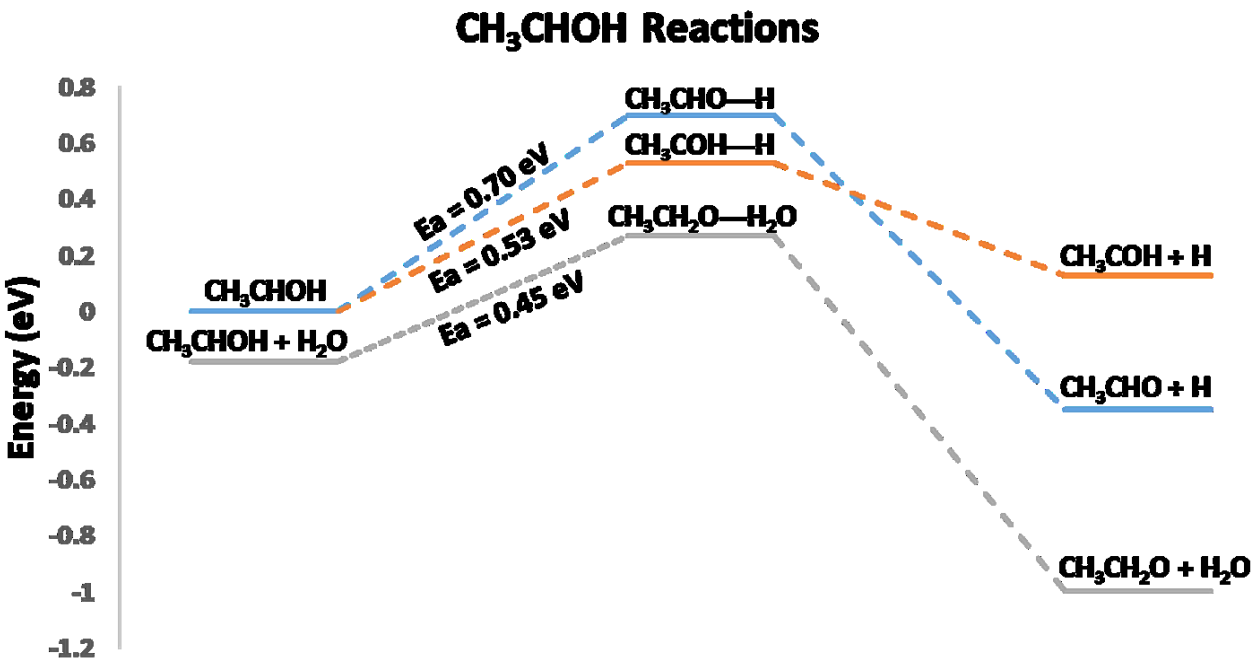

Figure 7: Potential energy landscape for the reactions emanating from CH_3CHOH.

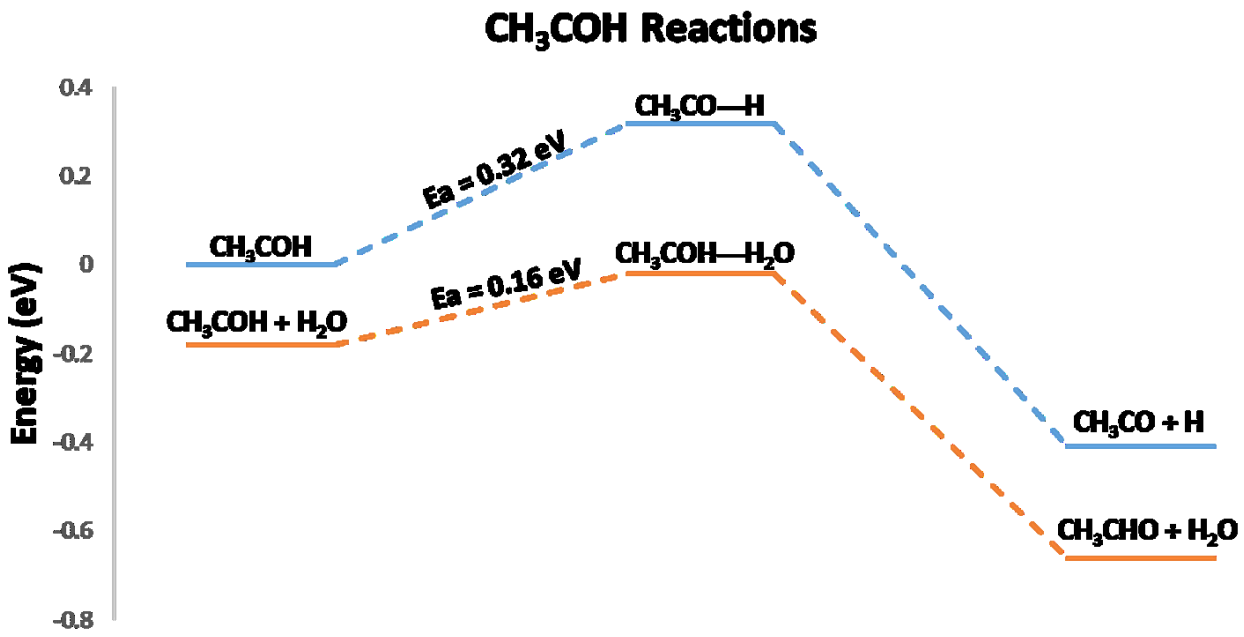

Figure 8: Potential energy landscape for the reactions emanating from CH_3COH.

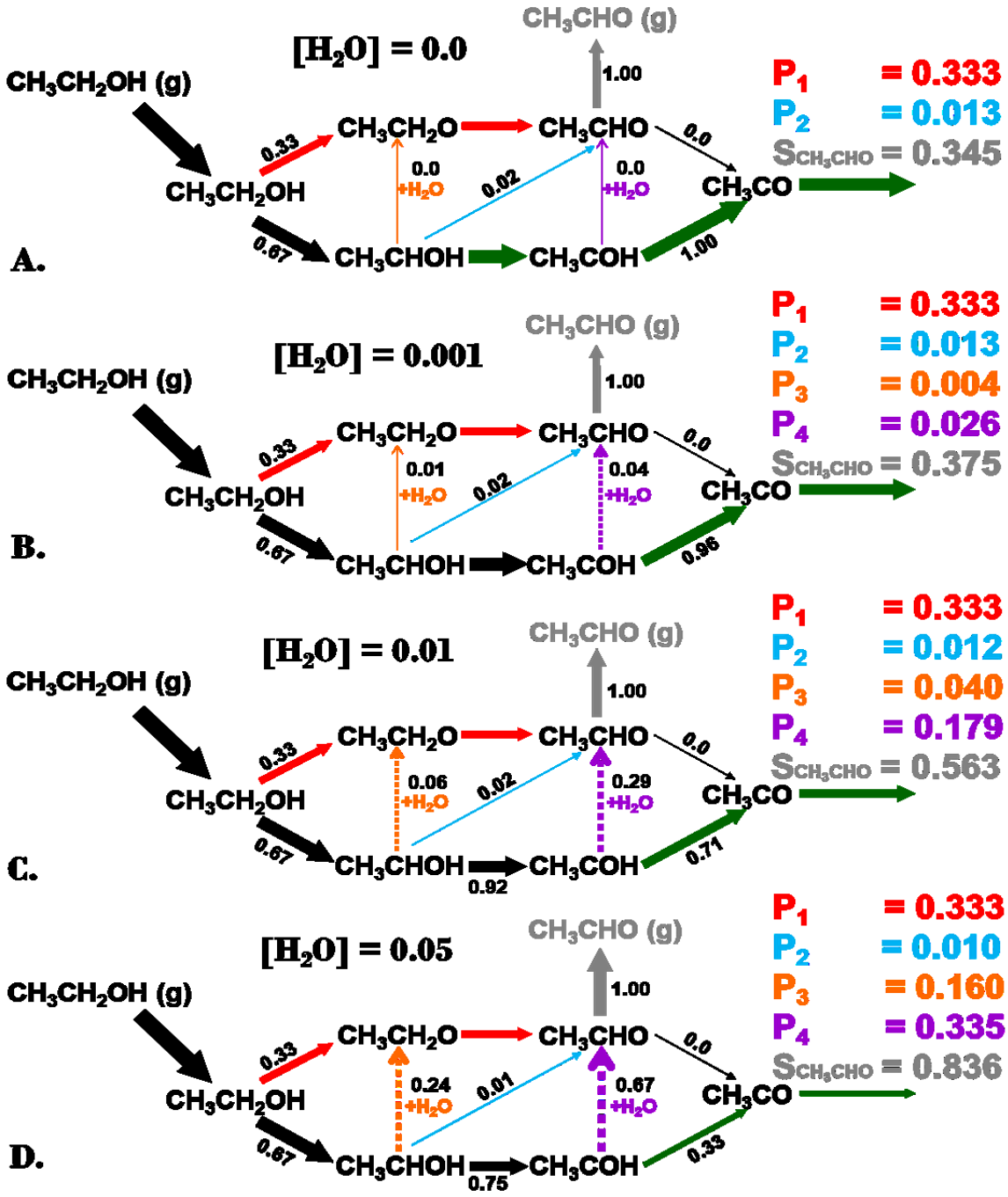

Figure 9: Kinetic study of acetaldehyde production vs. water coverage. The pathway probabilities (P_i) for the four pathways are given as well as the selectivity for acetaldehyde production (S_{CH_3CHO}). The water coverage ranges from 0.0 ML in panel A, 0.001 ML in panel B, 0.01 ML in panel C, and 0.05 ML in panel D. The quantities labeling the reactions are the branching ratios Γ_j^i.

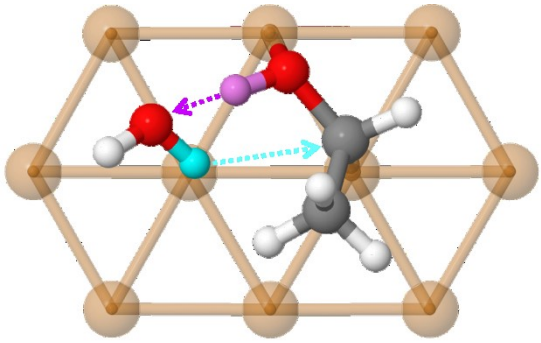

TOC Graphic